

PAPER

# Dynamical coupling of plasmons and molecular excitations by hybrid quantum/classical calculations: time-domain approach

To cite this article: Arto Sakko *et al* 2014 *J. Phys.: Condens. Matter* **26** 315013

View the [article online](#) for updates and enhancements.

## Related content

- [Surface plasmon resonance in gold nanoparticles: a review](#)  
Vincenzo Amendola, Roberto Pilot, Marco Frasconi *et al*.
- [Attosecond physics at the nanoscale](#)  
M F Ciappina, J A Pérez-Hernández, A S Landsman *et al*.
- [Experimental and theoretical studies of plasmon–molecule interactions](#)  
Hanning Chen, George C Schatz and Mark A Ratner

## Recent citations

- [The collective excitations and static dipole polarizability in small nanoparticles](#)  
J. A. Leiro
- [Capturing Plasmon–Molecule Dynamics in Dye Monolayers on Metal Nanoparticles Using Classical Electrodynamics with Quantum Embedding](#)  
Holden T. Smith *et al*
- [Real-Time Description of the Electronic Dynamics for a Molecule Close to a Plasmonic Nanoparticle](#)  
Silvio Pipolo and Stefano Corni



**IOP | ebooks™**

Bringing you innovative digital publishing with leading voices to create your essential collection of books in STEM research.

Start exploring the collection - download the first chapter of every title for free.

# Dynamical coupling of plasmons and molecular excitations by hybrid quantum/classical calculations: time-domain approach

Arto Sakko<sup>1</sup>, Tuomas P Rossi<sup>1</sup> and Risto M Nieminen<sup>2</sup>

<sup>1</sup> COMP Centre of Excellence, Department of Applied Physics, Aalto University School of Science, FI-00076 AALTO, Finland

<sup>2</sup> COMP Centre of Excellence, Department of Applied Physics and Dean's Office, Aalto University School of Science, FI-00076 AALTO, Finland

E-mail: [arto.sakko@aalto.fi](mailto:arto.sakko@aalto.fi)

Received 20 February 2014, revised 4 June 2014


Accepted for publication 9 June 2014

Published 16 July 2014

## Abstract

The presence of plasmonic material influences the optical properties of nearby molecules in untrivial ways due to the dynamical plasmon-molecule coupling. We combine quantum and classical calculation schemes to study this phenomenon in a hybrid system that consists of a Na<sub>2</sub> molecule located in the gap between two Au/Ag nanoparticles. The molecule is treated quantum-mechanically with time-dependent density-functional theory, and the nanoparticles with quasistatic classical electrodynamics. The nanoparticle dimer has a plasmon resonance in the visible part of the electromagnetic spectrum, and the Na<sub>2</sub> molecule has an electron-hole excitation in the same energy range. Due to the dynamical interaction of the two subsystems the plasmon and the molecular excitations couple, creating a hybridized molecular-plasmon excited state. This state has unique properties that yield e.g. enhanced photoabsorption compared to the freestanding Na<sub>2</sub> molecule. The computational approach used enables decoupling of the mutual plasmon-molecule interaction, and our analysis verifies that it is not legitimate to neglect the backcoupling effect when describing the dynamical interaction between plasmonic material and nearby molecules. Time-resolved analysis shows nearly instantaneous formation of the coupled state, and provides an intuitive picture of the underlying physics.

Keywords: plasmonics, metal-molecule interactions, computational electrodynamics, density functional theory, multiscale methods, nanotechnology

 Online supplementary data available from [stacks.iop.org/JPhysCM/26/315013/mmedia](http://stacks.iop.org/JPhysCM/26/315013/mmedia)

(Some figures may appear in colour only in the online journal)

## 1. Introduction

Plasmonic nanostructures attract wide interest in present-day science and technology. With precisely controlled design, they enable confining, guiding, and processing light in sub-wavelength structures [1, 2], and are thereby used in surface-enhanced spectroscopies [3], gas sensors [4],

photovoltaics [5], and in combining optical devices with molecular electronics [6, 7]. The coupling of quantum emitters with well-defined plasmonic structures even provides methods for optically controlled quantum information processing and for realizing novel optoelectronic devices [8, 9]. The developments in electron-beam lithography, self-assembly, and other nanofabrication techniques make it now

possible to create these optically functional materials with sub-nm details [10, 11].

Ultimately, the optical properties of all materials derive from their quantum-mechanical response to the perturbing light. Full quantum-mechanical treatment would be desirable for predicting the characteristics of nanoscale systems, but the significant computational cost of the electronic structure calculations makes them impractical already for relatively small systems [12]. Quantum-mechanical simulations have nevertheless been performed for model plasmonic systems, such as metallic surfaces, nanospheres and nanowires [13–16]. These studies have elucidated the quantum origins of the optical properties [17–22] of nanostructures and paved the way for including the relevant quantum effects in classical electrodynamical (ED) simulations [16, 21, 23, 24].

The crucial role of quantum effects is evident in the case of plasmon-molecule coupling. Depending on the metal and the molecule, this phenomenon can yield interesting changes in the system, such as enhanced molecular response properties [25], Fano-type resonances [26] and optical transparency [22]. For simulating the dynamical metal-molecule interaction in such hybrid systems one can treat the metal classically and the molecule using a quantum mechanical description [25–29]. The calculations provide insight into the coupling mechanism which is also linked to the chemical and electrodynamical enhancement mechanisms behind the surface-enhanced Raman scattering (SERS) and other plasmon-enhanced spectroscopies [3, 30–34]. To investigate these effects, many works have treated the quantum part of the system with the few-level approximation [22, 26, 35, 36]. However, the most accurate description of physisorbed molecules typically requires considering the full atomistic structure. Such calculations have been presented as well, but they mainly use frequency space approaches or are designed for SERS [25, 27–29, 34, 37, 38]. More method development is therefore necessary for simulating the time-dependent processes in transient spectroscopy, waveguiding, and plasmon-driven chemistry.

In this work we employ a recently proposed general strategy where the finite-difference time-domain (FDTD) method describes classical electrodynamics, and the time-dependent density-functional theory (TDDFT) the quantum physics [39, 40]. We show that this approach can tackle the dynamical coupling in plasmon-molecule systems. We use it to simulate the enhanced photoabsorption of molecules in the vicinity of metallic nanoparticles. The formation of hybrid plasmon-molecular states [41, 42] is also investigated, and analysis of the back-coupling mechanism as well as the time-resolved dynamics of the excited state evolution is presented. We also report the implementation of the method in the freely available real-space electronic structure code GPAW [43, 44]. Atomic units  $\hbar=m_e=e=1$  are used throughout this work, except for most numerical values that are given in electron volts and nanometers.

The structure of the paper is as follows. In section 2 we review the main parts of the computational approach and its implementation in the GPAW code. The calculations are presented in section 3. There we apply the method for studying the coupling of classical metallic nanoparticles with quantum-mechanically treated  $\text{Na}_2$  molecules. These calculations

demonstrate enhanced absorption of the molecules in the plasmonic ‘hot spots’ and the emergence of hybrid plasmon-molecule states. We also observe shifts in the energy levels of the hybrid states, which resemble the changes that are detected in the case of strong molecule-plasmon coupling [9, 41]. Finally we present a time-domain investigation of the formation of the coupled state, which reveals the relevant time scales and provides a new way to look at the coupling and enhancement mechanisms. The work is concluded in section 4.

## 2. Method

The optical properties of all materials depend on how they respond (absorb and scatter) to external electromagnetic fields. In classical electrodynamics, this response is described by the Maxwell equations. One widely used method for solving them numerically is the finite-difference time-domain (FDTD) approach [45, 46]. It is based on propagating the electric and magnetic fields in time under the influence of an external perturbation (light) in such a way that the observables are expressed in real space grid points. The optical constants are then obtained by analyzing the resulting far-field pattern. In the microscopic limit of classical electrodynamics the quasistatic approximation [47] is valid and an alternative set of time-dependent equations for the polarization charge, polarization current, and the electric field can be derived [39]. This quasistatic formulation of FDTD (QSFDTD) has advantageous features for nanoplasmonic calculations. The magnetic field is negligible and only the longitudinal electric field need to be considered, so that the number of degrees of freedom is decreased. Because the retardation effects and propagating solutions are excluded, longer time steps and a simpler treatment of the boundary conditions can be used. The method also provides a straightforward way to couple classical ED with electronic structure calculations through a common electric potential [40, 48].

Following the framework of [39], the classical polarization in the QSFDTD method is handled using the auxiliary differential equation approach. In each point  $\mathbf{r}$  of the uniform real space grid, the permittivity is written as

$$\epsilon(\mathbf{r}, \omega) = \epsilon_\infty + \sum_j \frac{\epsilon_0 \beta_j(\mathbf{r})}{\bar{\omega}_j^2(\mathbf{r}) - i\omega\alpha_j(\mathbf{r}) - \omega^2}, \quad (1)$$

where  $\alpha_j$ ,  $\beta_j$ ,  $\bar{\omega}_j$ , and  $\epsilon_\infty$  are fitting parameters used to match the experimental permittivity of the bulk material, and  $\omega$  is the frequency. In this work we have  $\epsilon_\infty = \epsilon_0$  for the high-frequency permittivity, but this condition is not obligatory [49]. In QSFDTD one propagates the polarization density  $\mathbf{P}(\mathbf{r}, t)$  and the polarization current density  $\mathbf{J}(\mathbf{r}, t)$ , which are nonzero only inside the metal. The other ingredients of the method, which are deduced from  $\mathbf{P}$  and  $\mathbf{J}$ , are the classical charge density  $\rho^{\text{cl}}(\mathbf{r}, t)$ , the electric potential  $V^{\text{cl}}(\mathbf{r}, t)$ , and the electric field  $\mathbf{E}(\mathbf{r}, t)$ . First, the charge density, which consists of the classical ( $\rho^{\text{cl}}(\mathbf{r}, t)$ ) and the quantum ( $\rho^{\text{qm}}(\mathbf{r}, t)$ ) contributions, determines the electric potential through the Poisson equation

$$\nabla^2 V^{\text{tot}}(\mathbf{r}, t) = -4\pi[\rho^{\text{cl}}(\mathbf{r}, t) + \rho^{\text{qm}}(\mathbf{r}, t)]. \quad (2)$$

The electric field is then

$$\mathbf{E}(\mathbf{r}, t) = -\nabla V^{\text{tot}}(\mathbf{r}, t). \quad (3)$$

The time-propagation scheme for  $\mathbf{P}(\mathbf{r}, t)$  and  $\mathbf{J}(\mathbf{r}, t)$  follows from the continuity equation and the connection between  $\mathbf{P}(\mathbf{r}, t)$ ,  $\mathbf{J}(\mathbf{r}, t)$ , and  $\epsilon(\mathbf{r}, \omega)$  [39].

The quantum-mechanical charge density  $\rho^{\text{qm}}(\mathbf{r}, t)$  can be solved using various electronic structure calculation methods. In the Kohn–Sham density functional theory scheme (KS-DFT), the electronic structure is solved for the KS-orbitals  $\phi_i(\mathbf{r})$ , which determine the electron density as  $\rho^{\text{qm}}(\mathbf{r}) = \sum_i f_i |\phi_i(\mathbf{r})|^2$ , where  $f_i$  are the occupation numbers ( $f_i = 2$  for a typical spin-unpolarized calculation). The ground state KS-equation is

$$\left[ -\frac{1}{2} \nabla^2 + V^{\text{tot}}(\mathbf{r}) + V^{\text{xc}}(\mathbf{r}) + V^{\text{ext}}(\mathbf{r}) \right] \phi_j(\mathbf{r}) = \epsilon_j \phi_j(\mathbf{r}), \quad (4)$$

where the exchange-correlation potential  $V^{\text{xc}}[\rho^{\text{qm}}](\mathbf{r})$  includes the complicated many-body effects of the electron-electron interaction in an approximate manner, and  $V^{\text{ext}}(\mathbf{r})$  is the external potential. The electric and exchange-correlation potentials depend on the electron density, and therefore equation (4) is solved self-consistently.

The time evolution of the KS-orbitals follows the equation

$$\left[ -\frac{1}{2} \nabla^2 + V^{\text{tot}}(\mathbf{r}, t) + V^{\text{xc}}(\mathbf{r}, t) + V^{\text{ext}}(\mathbf{r}, t) \right] \phi_j(\mathbf{r}, t) = i \frac{\partial \phi_j(\mathbf{r}, t)}{\partial t}, \quad (5)$$

as was proven by Runge and Gross [50]. The numerical implementation of the time propagation is realized in GPAW using the methods described in [43, 51].

The GPAW computer code employs a uniformly distributed real-space grid for expressing the wavefunctions, densities, potentials, and the differential operators [52]. The projector augmented wave (PAW) method is used for freezing the inert core electrons in the calculation and thereby decreasing the computational cost significantly [53]. In practice this means that one solves equations (4) and (5) for the smooth valence pseudo-wavefunctions and then the all-electron density can be deduced by the well-established PAW transformation [44, 54].

Our implementation of QSFDTD benefits from the advanced numerical features of the GPAW code, e.g. efficient parallelization techniques. The Poisson equation (equation (2)) is solved in such a way that the quantum and classical electric potentials are determined in separate grids that can have different spacings. The spacing of the coarser classical grid is restricted to be  $2^n$  times the spacing of the denser quantum grid, where  $n$  is an integer. Then some grid points are shared by the two grids, and for the rest of the points in the overlapping regime the values of the potential and the density are calculated using an interpolation routine. Although the number of degrees of freedom in the simulation is large, the advantage of the used real-space methods (both FDTD and TDDFT) is good parallelizability that follows from the local nature of the relevant algebraic operations.

The metal-molecule interaction can be divided into static and dynamical parts [30, 31]. The static interaction includes the formation of chemical bonds between surface and the molecule, as well as the electrostatic polarization of the metal by the molecule [55]. Since the formation of chemical bonds is an inherently quantum-mechanical effect, including it in the calculation would require electronic structure calculations of the metal as well. In plasmonic structures the dynamical interaction is usually more important than the static effects, because of the strong charge oscillation and electric field associated with the plasmon. In this work we focus solely on the dynamical effects and start the time evolution from the vacuum ground state of the molecule. To achieve this, the condition  $\epsilon(\omega=0) = \epsilon_0$  is enforced by adding an extra oscillator ( $\alpha = 0.10$  eV,  $\beta = 0.01$  eV,  $\bar{\omega} = 0.01$  eV) in the permittivity (equation (1)). Such a low-energy oscillator is non-negligible only near  $\omega=0$ , so that  $\epsilon(\omega)$  and thereby the dynamical response of the coupled system remains intact in the optical energy range. In the ground state calculation the additional oscillator prevents the polarization of the system and provides a well-defined starting point for the time evolution.

The photoabsorption spectrum is extracted from the time-propagation simulations with the framework that was originally presented in [56]. The system is in the ground state in the beginning of the time propagation, and at time  $t=0$  an external field  $\mathbf{E}(\mathbf{r}, t) = E_0 \hat{\mathbf{x}} \delta(t)$  is applied, where  $E_0$  is sufficiently small so that the nonlinear effects can be neglected in the analysis. This perturbation corresponds to a perfect white laser, i.e., all frequencies are included with an equal weight. The perturbation excites the system via dipole transitions, and therefore the charge density starts to fluctuate in time. The fluctuations are strongest at the resonance frequencies of the system (e.g. the plasmon frequency), and the photoabsorption cross section  $\sigma^{\text{abs}}(\omega)$  is calculated from the time-dependent dipole moment

$$\boldsymbol{\mu}(t) = \boldsymbol{\mu}^{\text{qm}}(t) + \boldsymbol{\mu}^{\text{cl}}(t) = \int d^3\mathbf{r} \, \mathbf{r} \rho^{\text{qm}}(\mathbf{r}, t) + \int d^3\mathbf{r} \, \mathbf{P}(\mathbf{r}, t) \quad (6)$$

via the connection  $\sigma^{\text{abs}}(\omega) = \frac{4\pi\omega}{c} \text{Im}(\delta\mu_x(\omega)/E_0)$ , where  $\delta\mu_x$  is the induced dipole moment. Instead of the photoabsorption cross section we present the dipole strength function

$$S(\omega) = \frac{c}{2\pi^2} \sigma^{\text{abs}}(\omega) = \frac{2\omega}{\pi} \text{Im}(\delta\mu_x(\omega)/E_0) \quad (7)$$

which satisfies the sum rule  $\int_0^\infty d\omega S(\omega) = N_{\text{el}}$ , i.e., it integrates to the number of valence electrons [43].

In addition to the dipole moment and photoabsorption spectrum, we present results for the induced charge density and the electric field distributions for the plasmon modes. These quantities are relevant for visualizing and characterizing the plasmons in molecules and nanostructures, as well as for understanding the near-field enhancement in the vicinity of metallic nanoparticles [57–59]. The charge density fluctuations at each frequency induce a time-dependent Hartree potential via  $\nabla^2 V^{\text{tot}}(\mathbf{r}, \omega) = -4\pi\rho^{\text{tot}}(\mathbf{r}, \omega)$  which then determines the electric near-field as  $\mathbf{E}(\mathbf{r}, \omega) = -\nabla V^{\text{tot}}(\mathbf{r}, \omega)$ .



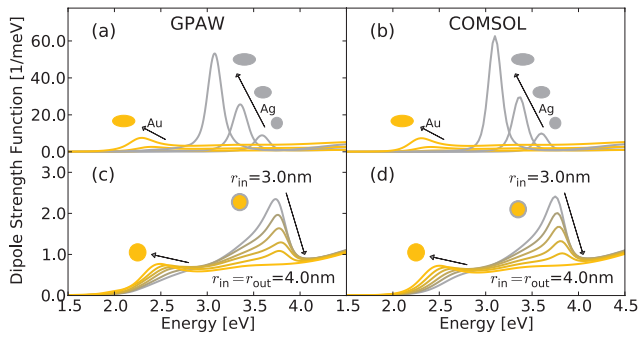


**Figure 1.** The photoabsorption spectrum of nanoellipsoids (*a*, *b*) and Au/Ag core-shell nanospheres (*c*, *d*) calculated with the QSFDTD method using the new GPAW implementation (*a*, *c*) and with the full Maxwell equations using the COMSOL software (*b*, *d*). Gray and yellow colors denote silver and gold, respectively.

### 3. Calculations

For the QSFDTD part of the calculations, the used parametrizations for the permittivity of gold and silver were obtained from [39]. The adiabatic local density approximation was used to include the exchange and correlation effects in TDDFT. The orthorhombic simulation box was generated in such a way that the separation between the simulation box boundaries and the classical materials was at least 2 nm. For the fully classical calculations (presented in figure 1) the spacing between the grid points was 0.16 nm, the time evolution was followed for 30 fs using time steps of 20 as, and the presented spectra were convoluted with Gaussian lineshape using the full width at half maximum (FWHM) of 0.23 eV. For the hybrid quantum/classical calculations (presented in figures 3–4 and 6–10), the grid spacings for the KS-orbitals and classical charge polarization were 0.04 nm and 0.08 nm, respectively, and the distance between the atoms and the grid borders was 0.6 nm. In these calculations the time evolution was followed for 15 fs with 20 as time steps, and the spectra were convoluted with Gaussian FWHM of 0.47 eV. The calculation scripts are included in the supplementary material ([stacks.iop.org/JPhysCM/26/315013/mmedia](http://stacks.iop.org/JPhysCM/26/315013/mmedia)).

#### 3.1. Classical nanoellipsoids and core-shell spheres

The computational methods in nanoplasmonics must be able to describe the geometrical effects and the plasmon hybridization, because these properties are behind the operation and tunability of nanoplasmonic devices. QSFDTD is known to correctly predict the photoabsorption spectrum of metallic nanospheres and nanosphere dimers, as well as the hot spots between two nearly touching nanoparticles [39]. Here we extend these investigations and study how the system geometry and the presence of multiple metals influences the positions and intensities of the plasmon peaks. In order to do that, we compare the predictions of our QSFDTD implementation in GPAW against full Maxwell calculations that were performed with the COMSOL software<sup>3</sup>.

Our first test set consists of metallic (Au and Ag) nanoellipsoids, whose short axis is fixed to 8 nm and the long axis are

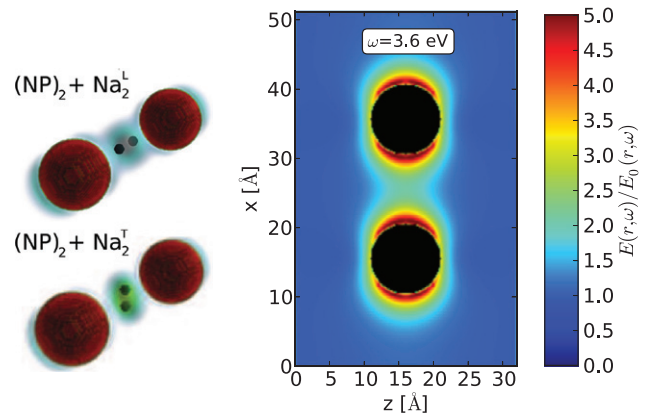


**Figure 2.** Schematic view of the Na<sub>2</sub> molecule located in the gap between two metallic nanoparticles in longitudinal (top) and transversal (bottom) orientations. The electric near field in the vicinity of the nanoparticles is shown on the right.

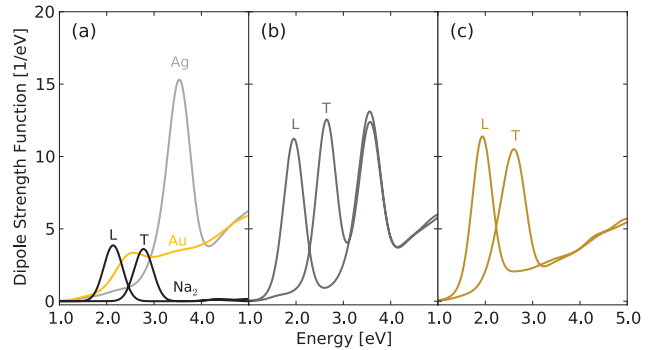


**Figure 3.** Photoabsorption spectra of (*a*) freestanding nanoparticle dimer and Na<sub>2</sub> molecule, (*b*) silver nanoparticle dimer dynamically coupled with Na<sub>2</sub> molecule, and (*c*) gold nanoparticle dimer dynamically coupled with Na<sub>2</sub> molecule.

8 nm, 12 nm, and 16 nm. The perturbing electric field is polarized along the elongated axis, so that the geometrical effect is emphasized. The results are presented in figures 1(*a*) and (*b*), which clearly show that our QSFDTD implementation reproduces the main features of the full solutions. In particular the plasmon redshift as the system is elongated is evident, and also the plasmon intensity agrees well with the COMSOL calculation.

The second test system is a layered metal sphere (gold core with silver shell), which has a diameter of 8 nm and whose Au:Ag ratio is varied. The results are shown in figures 1(*c*) and (*d*). The overall agreement is very good, and all main features are reproduced by the QSFDTD method. The photoabsorption spectra contain one peak originating from the gold plasmon (around 2.5 eV) and another one from the silver plasmon (around 3.7 eV). The former is significantly broad due to the strong interband damping that takes place when the plasmon overlaps in energy with the d-electron excitations. The onset energy for the d-band transitions in Au and Ag are 2.3 eV and 3.9 eV, i.e. below and above the LSPR frequency, respectively [60]. The calculated spectra show that the silver plasmon blueshifts and gold plasmon redshifts with

<sup>3</sup> RF module of the COMSOL software; [www.comsol.com](http://www.comsol.com).

the increasing size of the gold core. These observations are in good agreement with the experimental results for larger but otherwise similar core-shell clusters [61].

The aforementioned calculations confirm the performance of the QSFDTD approach for small systems. They validate our implementation and justify its use for the nanoscale classical electrodynamics simulations where geometrical effects are relevant. Furthermore, because both QSFDTD and TDDFT are now known to work with good accuracy, they can be merged together into the hybrid method that was described before. This new feature is utilized for the rest of the calculations.

### 3.2. Photoabsorption of $\text{Na}_2$ coupled with classical nanoparticle dimer

Here the new implementation is used to propagate the classical and quantum-mechanical subsystems simultaneously. The studied system, illustrated in figure 2, consists of two spherical nanoparticles (silver or gold, diameter of 1 nm) and a  $\text{Na}_2$  molecule that is located between them. The structure is similar to the ones in [22, 35 and 36], but in our case the molecule is treated atomistically with TDDFT instead of a few-level system.  $\text{Na}_2$  molecule is chosen for our calculations because its resonance frequencies are close to the plasmon frequencies of silver and gold nanoparticles. Sodium atom chains are generally ideal model systems for plasmonic studies due to their relatively simple electronic structure and the tunability of the optical excitation energies by changing the chain length and the interatomic distance [62, 63]. In our calculations we use the bond length of 0.308 nm. Two different orientations of the molecule are studied: in the first, longitudinal case the Na-Na bond is parallel to the interparticle gap ( $(\text{NP})_2 + \text{Na}_2^{\parallel}$ ), and in the second, transversal case it is perpendicular to the gap ( $(\text{NP})_2 + \text{Na}_2^{\perp}$ ). In all calculations the size of the gap is 1 nm, and the perturbing electric field is oriented parallel to it.

The calculated photoabsorption spectra of the freestanding  $\text{Na}_2$  and the nanoparticle dimer are presented in figure 3(a). The spectra show a strong polarization dependence of the  $\text{Na}_2$  excitations, as well as the hybridized plasmon resonance of the nanoparticles. In the longitudinal direction the main resonance of  $\text{Na}_2$  occurs at 2.1 eV and has peak intensity of  $3.9 \text{ eV}^{-1}$ . The transversal resonance occurs at 2.8 eV, and its peak intensity is  $3.6 \text{ eV}^{-1}$ . These excitations are significantly weaker than the plasmon of the silver nanoparticle dimer, which appears at 3.6 eV. The plasmon resonance of gold is not as strong due to the interband damping, and its frequency 2.5 eV is close to the transversal resonance frequency of  $\text{Na}_2$ .

The photoabsorption spectrum of the combined system is shown in figures 3(b) and (c). With silver nanoparticles, two peaks appear in both orientations of the molecule. Based on their energies, the one at the lower energy is assigned as the molecular excitation, and the higher energy one as the hybridized nanoparticle plasmon. Due to the interaction of the two subsystems, these excitations are rather different compared to the ones in the freestanding case. The most prominent difference is the stronger photoabsorption of the molecular resonances. The enhancement is a general property of the

molecules in the vicinity of nanoscale plasmonic materials, and follows from the strong intensity of the plasmonic near-field. This phenomenon is utilized in various surface-, nanoparticle-, and tip-enhanced spectroscopies [4, 64–67].

The photoabsorption enhancement is evident also in the case of gold nanoparticles. In contrast to the case with silver nanoparticles, the gold plasmon cannot be resolved because it is suppressed and merged with the molecular excitation. The results show that gold and silver nanoparticles are nearly equally strong photoabsorption amplifiers in this case. We also note that the magnitude of the intensity enhancement of both the longitudinal and the transversal excitations is almost equal.

A desirable feature in all surface-enhanced and related spectroscopies is that the electric near field of NPs should be maximized in the regions where the molecules of interest are located. Sharper tips, larger structures, and narrow regions typically yield the strongest hot spots. To demonstrate this geometry dependence both on the electric field enhancement and on the photoabsorption cross section, we study the absorption spectrum of the  $\text{Na}_2$  molecule in L-orientation as a function of the diameter of the two surrounding silver nanoparticles. The results are presented in figure 4, where a strong diameter dependence can be observed. The inset also shows the values of the field enhancement in the center of the NP gap, as well as the intensity enhancement of the longitudinal resonance peak. The field is amplified also when the external field frequency is 2.0 eV, i.e., below the plasmon frequency 3.6 eV, although the effect is stronger at the resonance. The electric near-field and the photoabsorption intensities increase linearly and quadratically as a function of the NP diameter, respectively. This behaviour is due to the mutual back-coupling effect that is discussed below.

In addition to the enhanced photoabsorption, the calculations also show molecular peaks redshifting by 0.1–0.2 eV. Also the silver plasmon slightly moves towards higher energies. The interaction apparently pushes the lower energy resonance downward in energy, and the higher energy resonance upwards. In the strong coupling regime this tendency is pronounced and yields an avoided crossing type feature [41]. Calculations of strongly coupled metal-emitter states have been presented e.g. in [36]. In our case we do not expect the states to be strongly coupled, because they do not overlap in energy and also because the plasmon linewidth is relatively large. The induced densities at the resonance frequencies are presented in figure 5. They show how the molecular and plasmonic excitations are coupled and lead to hybridized molecular-plasmonic states.

### 3.3. Back-coupling effects

Next we analyze in more detail the dynamical coupling between the classical and quantum subsystems. Phenomenological models of the coupling have shown that the back-coupling through the dynamical image field effect is crucial for the accurate treatment of the effective polarizability of molecules when they are adsorbed on metal surfaces [30]. We analyze

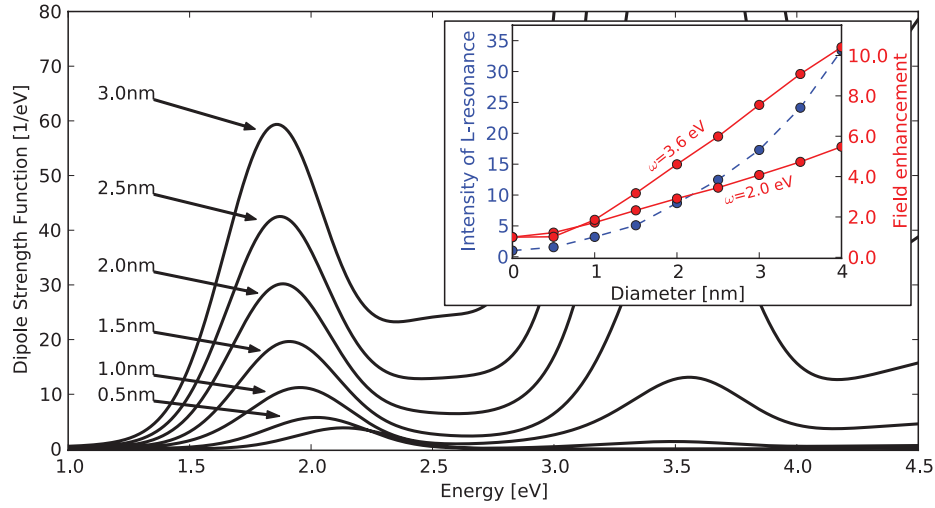


**Figure 4.** The photoabsorption spectrum of  $(\text{AgNP})_2 + \text{Na}_2$  with varying nanoparticle diameter (annotated with the arrows). The inset shows the values of the electric near-field enhancement in the center of the gap at the frequencies that correspond to the molecular (2.0 eV) and plasmonic (3.6 eV) resonances (solid red curves), as well as the molecular L-resonance peak intensity with respect to the freestanding case (blue dashed curve).

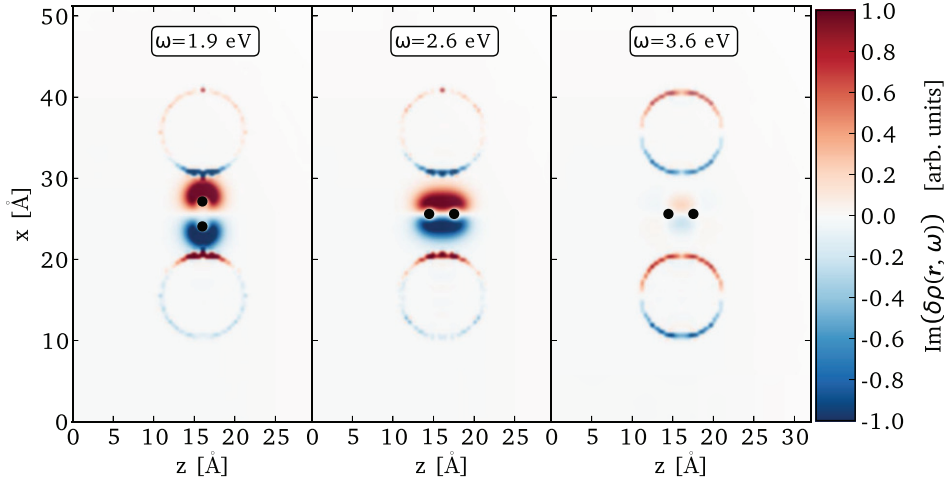


**Figure 5.** The imaginary parts of the induced charge densities associated with the hybrid excited states that form when  $\text{Na}_2$  is located in the gap between two silver nanoparticles.

this phenomenon by separating the Poisson equation (equation (2)) into two parts:

$$\begin{aligned} \nabla^2 V^{\text{qm}}(\mathbf{r}, t) &= -4\pi[\rho^{\text{qm}}(\mathbf{r}, t)] \\ \nabla^2 V^{\text{cl}}(\mathbf{r}, t) &= -4\pi[\rho^{\text{cl}}(\mathbf{r}, t)], \end{aligned} \quad (8)$$

so that the total electric potential is  $V^{\text{tot}}(\mathbf{r}, t) = V^{\text{cl}}(\mathbf{r}, t) + V^{\text{qm}}(\mathbf{r}, t)$  and the electric field is  $\mathbf{E}(\mathbf{r}, t) = \mathbf{E}^{\text{cl}}(\mathbf{r}, t) + \mathbf{E}^{\text{qm}}(\mathbf{r}, t) = -\nabla V^{\text{cl}}(\mathbf{r}, t) - \nabla V^{\text{qm}}(\mathbf{r}, t)$ . To obtain insight into the coupling process, the partial potentials  $V^{\text{cl}}(\mathbf{r}, t)$  and  $V^{\text{qm}}(\mathbf{r}, t)$  can be used to make the classical system experience the electric field of the quantum system but not the other way around. Then the electric field that yields classical polarization is

$$\mathbf{E}(\mathbf{r}, t) = -\nabla V^{\text{cl}}(\mathbf{r}, t) - \nabla V^{\text{qm}}(\mathbf{r}, t) \quad (9)$$

as usual, but the quantum-mechanical Kohn–Sham equation is

$$\begin{aligned} \left[ -\frac{1}{2}\nabla^2 + V^{\text{qm}}(\mathbf{r}, t) + V^{\text{xc}}(\mathbf{r}, t) + V^{\text{ext}}(\mathbf{r}, t) \right] \phi_j(\mathbf{r}, t) \\ = i \frac{\partial \phi_j(\mathbf{r}, t)}{\partial t} \end{aligned} \quad (10)$$

In the opposite half-coupling scheme, the quantum system experiences the usual potential including the classical charge polarization, but the classical part does not see the quantum subsystem:

$$\mathbf{E}(\mathbf{r}, t) = -\nabla V^{\text{cl}}(\mathbf{r}, t), \quad (11)$$

$$\begin{aligned} \left[ -\frac{1}{2}\nabla^2 + V^{\text{cl}}(\mathbf{r}, t) + V^{\text{qm}}(\mathbf{r}, t) + V^{\text{xc}}(\mathbf{r}, t) + V^{\text{ext}}(\mathbf{r}, t) \right] \\ \times \phi_j(\mathbf{r}, t) = i \frac{\partial \phi_j(\mathbf{r}, t)}{\partial t} \end{aligned} \quad (12)$$

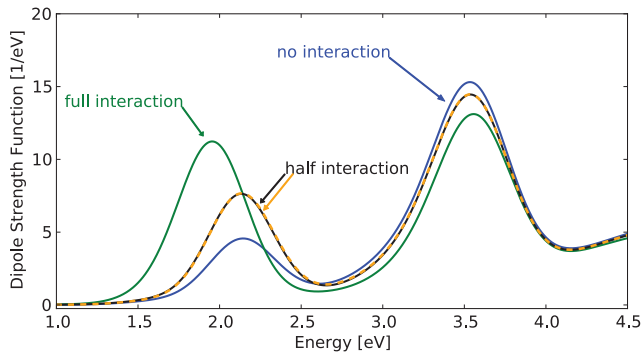


**Figure 6.** The photoabsorption spectra of  $(\text{AgNP})_2 + \text{Na}_2^L$  when calculated with four different interaction schemes, see text for details.

The photoabsorption spectra of such calculations for the longitudinally oriented  $\text{Na}_2$  molecule between two silver nanoparticles are presented in figure 6. The result shows that in this case the coupling can be divided into two equally strong components: the solid black and dashed orange curves denoting the two half-coupling schemes are almost on top of each other. This behaviour is independent of the NP diameter in our calculations, which in this example case is 1 nm. Thus, both quantum-to-classical and classical-to-quantum interactions are equally important for the formation of the hybrid states, and the back-coupling effects can not be neglected. The mutual coupling is especially crucial for shifting the energy of the resonances, which is observed only when the full interaction is taken into account. Our results are in line with the general behaviour of metal-molecule systems: the presence of a plasmonic nanoparticle increases the molecule's effective polarizability due to the plasmon field and the back-coupling effect [30, 68].

### 3.4. Time-resolved study of $\text{Na}_2$ coupled with Ag nanoparticles

The employed time-domain approach also enables investigations from another perspective: following the time evolution of the coupled system yields an intuitive picture of the coupling mechanism and reveals the relevant time scales. The time-resolved studies of the electronic structure are also relevant for interpreting and designing ultrafast time-resolved spectroscopic experiments [69]. It is also very useful in identifying the weak and strong coupling regimes in the emitter-plasmon systems [35]. In figure 7 we show the time evolution of the dipole moments of classical and quantum subsystems after the initial perturbation, when the subsystems do not interact with each other (a) and when the interaction is included (b). The dashed blue and narrow yellow curves in figure 7 denote the quantum and classical subsystem contributions to the total dipole moment, respectively, and the thick green curve shows the total dipole moment of the system.

Comparison of figures 7(a) and (b) shows that the mutual interaction drives the oscillations of the subsystems into phase with each other and thereby leads to larger oscillation amplitude. This mechanism thereby explains both the previously

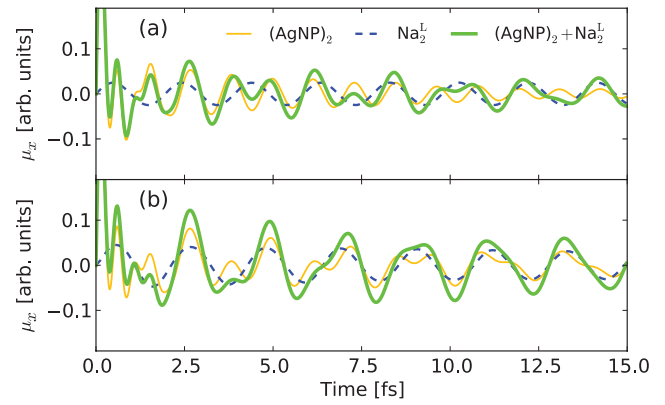


**Figure 7.** The time evolution of the dipole moments associated with the classical and quantum subsystems after the system has been excited by the external electric field at  $t=0$  fs. In (a) the subsystems do not interact and in (b) they interact.

discussed shifts in resonance energies as well as the enhanced photoabsorption cross section.

We also use the time-domain approach for analyzing how the coupling proceeds in time by using a numerical experiment where only one of the subsystems of  $(\text{Ag NP})_2 + \text{Na}_2$  is perturbed by the external field. Because of the mutual interaction, the perturbed subsystem starts to drive the unperturbed one, until an equilibrium is achieved so that the hybridized state is formed. The results for the time-dependent dipole moments are presented in figure 8. The solid black curve in figure 8(a) shows the dipole moment of the quantum subsystem after the classical subsystem is perturbed. For reference, the dashed blue curve shows the dipole moment of the quantum subsystem after perturbing both subsystems. Similarly, figure 8(b) shows the dipole moment of the classical subsystem after perturbing only the quantum subsystem (solid black curve) or the whole system (dashed yellow curve). The results indicate that the coupling takes place very fast: the dipole moment gets in phase with the reference case already during the first oscillation period. Also the amplitude saturates virtually without any delay.

A close look at figure 8 reveals that the classical plasmon and the molecular oscillations behave differently: in all cases both subsystems exhibit dipolar oscillations corresponding to the molecular L-resonance, but the classical plasmon oscillation is visible only in  $\mu_x^{\text{cl}}$  after the whole system is excited. In other words, the classical subsystem can excite the molecular oscillations, but not the other way around. The reason is that the classical charge oscillations have a significant electric field component at the molecular resonance frequency, as was shown in the inset of figure 4. This field inevitably excites the molecule and leads to the observed behaviour. The situation does not work the other way around: the excited molecule yields a negligible electric field component at the plasmon frequency, and therefore it can not excite the plasmon in the metal.

In addition to the time-dependent dipole moment, we also analyze how the energy flows in time between the classical and quantum subsystems. The time evolution of the total energy of  $\text{Na}_2$  molecule with respect to its ground state value is shown



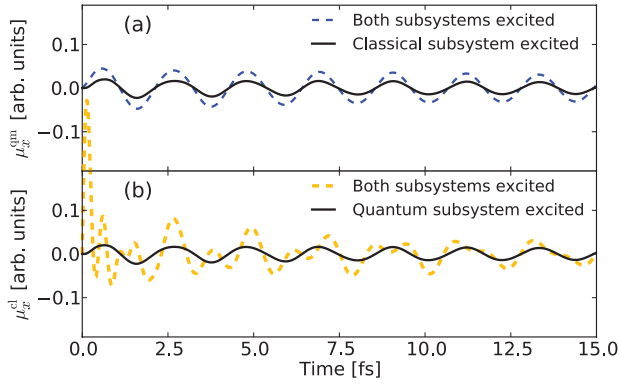


**Figure 8.** The time evolution of the dipole moment associated with (a) the quantum and (b) classical subsystems after either only one of the subsystems or both of them have been excited by an external electric field  $\mathbf{E}(\mathbf{r}, t) = E_0 \hat{\mathbf{e}}_x \delta(t)$ .

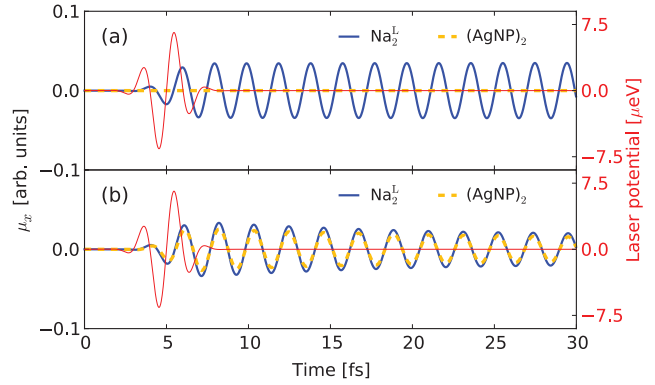


**Figure 10.** The time evolution of the dipole moments associated with the classical and quantum subsystems following an excitation of  $\text{Na}_2$  by an external laser pulse. In (a) the subsystems do not interact and in (b) they interact.

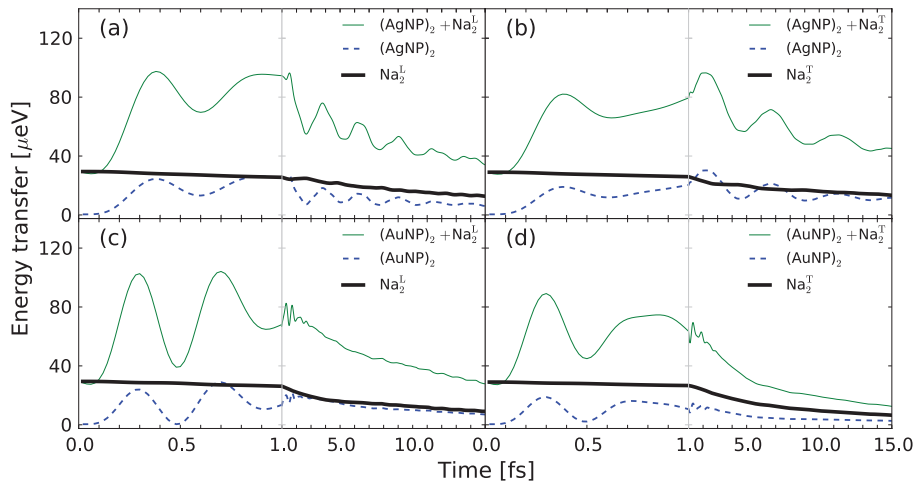


**Figure 9.** The time evolution of the transfer of energy from the classical plasmon and the external field to the quantum subsystem, after either one or both of the subsystems have been excited by the external electric field  $\mathbf{E}(\mathbf{r}, t) = E_0 \hat{\mathbf{e}}_x \delta(t)$ . The studied systems are (a)  $(\text{AgNP})_2 + \text{Na}_2^L$ , (b)  $(\text{AgNP})_2 + \text{Na}_2^I$ , (c)  $(\text{AuNP})_2 + \text{Na}_2^L$ , and (d)  $(\text{AuNP})_2 + \text{Na}_2^I$ .

in figure 9. When only the quantum subsystem is perturbed at  $t=0$  fs (thick black curves), the total energy decreases slowly and almost monotonically as the energy flows to the classical material, and the energy decays at the rate determined by the imaginary part of the metal's permittivity. If only the classical subsystem is perturbed (dashed blue curves), the energy is transferred to the quantum subsystem during the first 0.4 fs so that the molecular resonance is excited. After the early phase excitation, the energy continues oscillating and is transmitted to the classical material at the rate that depends on the structure. When the whole system is perturbed (narrow green curves), the total energy change is larger than the sum from the partial ones. The energy scale depends on the magnitude of the initial perturbation (here  $E_0=0.001$  a.u.), which was chosen to be very small so that nonlinear effects are not induced in the propagation.

The delta-pulse perturbation used in previous calculations is useful for calculating the (linear) response functions in time domain, but it is often advantageous to excite the system with external fields that have arbitrary temporal shape [43]. Such calculations simulate the actual time-resolved experiments

and can provide a more realistic picture of the underlying physics [69]. The previous observation of the nearly instantaneous coupling is also supported by a calculation where the molecule is excited by an ultrafast laser pulse. We choose a weak pulse that is resonant with the L-excitation of  $\text{Na}_2$  and apply it only to the quantum-mechanical subsystem. Figure 10 shows that when the subsystems ( $(\text{AgNP})_2$  and  $\text{Na}_2^L$ ) interact, the time evolutions of the dipole moments of the two subsystems are virtually identical from the beginning. This study of the coupling process also shows that in contrast to the non-interacting case (figure 10(a)), the oscillation amplitude in figure 10(b) decreases in time. The lifetime effects are not included in adiabatic TDDFT calculations, but the electrostatic coupling opens another decay channel through the imaginary part of the metal dielectric function.

#### 4. Conclusions and discussion

Combining quantum-mechanical and classical simulations is a challenging but important subject that is often encountered in multiscale modeling. In biomolecular physics and chemistry,

the chemical reactions can be simulated with the QM/MM scheme that merges the classical and quantum molecular dynamics simulations together [70]. Quantum effects must also be accounted for when designing circuits and devices in nanoscale and molecular electronics [71, 72]. An analogous need is now emerging in nano-optics where the traditional approaches that are based on solving Maxwell equations with local bulk permittivity are not sufficient for all realizable optical components [9]. The miniaturization of the optically functional devices, the increased experimental sensitivity, and the utilization of quantum phenomena require the simulation of the light-matter interaction also from the electronic structure point of view. The hybrid simulation method where FDTD and TDDFT schemes are combined has potential as a widely applicable method for a variety of nano-photonic phenomena: both methods are general and have been applied in numerous problems in electrodynamics, optics, molecular physics, spectroscopy, biophysics, and molecular electronics. In contrast to most alternative schemes, the combination of FDTD and TDDFT enables atomistic modeling of time-resolved phenomena.

The combination of FDTD and TDDFT can be used in a wide range of applications, but its limitations must be understood and taken into account. For instance, if the approach is combined with Ehrenfest molecular dynamics [73] and utilized for exploring plasmon-enhanced chemistry, one should consider the lack of forces between the classical part and the atoms in the molecular system. The method also inherits the limitations of TDDFT, so that its accuracy for excitonic and charge transfer systems depends on the chosen approximation for the exchange and correlation. Another limitation is that the dielectric permittivity is a linear response function, and our current implementation is not applicable in the case of such strong external fields that induce nonlinear effects in the classical system. Moreover, our scheme does not account for the radiative decay channel and the finite lifetime of the molecular excitations, which can also yield significant effects in the optical response [74].

In this work we implemented the QSFDTD+TDDFT scheme in the electronic structure computer code GPAW and used it for studying the dynamical coupling between classical and quantum subsystems. The emergence of hybrid molecular-plasmonic states, which have been experimentally observed [41, 42], was simulated for a Na<sub>2</sub> molecule that is placed between two metallic nanoparticles. The coupling between these subsystems was separated into two equally relevant components, implying that the back-coupling must not be neglected. The time-dependent dipole moments and the energy transfer between the subsystems showed that the coupling takes place immediately after the system is excited. The results shed light on the origins of the enhanced photo-absorption and spectral changes. The time-domain formalism will be useful for future studies in nano-optics, especially when atomistic and time-resolved simulations are of interest. This involves investigations of the strongly coupled plasmon-emitter systems [35], the excited-state molecular dynamics and chemical reactions [73] as well as the transient spectroscopies [69] in the presence of plasmonic nanoparticles.

## Acknowledgments

We thank Lauri Lehtovaara, Martti Puska, and Jussi Enkovaara for useful discussions. The Academy of Finland (Centres of Excellence Program) is acknowledged for the financial support, and Aalto Science-IT project and the Finnish IT Center for Science (CSC) for the computational resources. TPR acknowledges financial support from the Vilho, Yrjö and Kalle Väisälä Foundation.

## References

- [1] Maier S A, Kik P G, Atwater H A, Meltzer S, Harel E, Koel B E and Requicha A A G 2003 *Nature Mater.* **2** 229–32
- [2] Giannini V, Fernández-Domínguez A I, Heck S C and Maier S A 2011 *Chem. Rev.* **111** 3888–912
- [3] Willets K A and Van Duyne R P 2007 *Ann. Rev. Phys. Chem.* **58** 267–97
- [4] Bingham J M, Anker J N, Kreno L E and Van Duyne R P 2010 *J. Am. Chem. Soc.* **132** 17358–9
- [5] Pillai S and Green M A 2010 *Solar Energy Mater. Solar Cells* **94** 1481–6
- [6] Banerjee P, Conklin D, Nanayakkara S, Park T H, Therien M J and Bonnell D A 2010 *ACS Nano* **4** 1019–25
- [7] Tan S F, Wu L, Yang J K W, Bai P, Bosman M and Nijhuis C A 2014 *Science* **343** 1496
- [8] Savasta S, Saija R, Ridolfo A, Di Stefano O, Denti P and Borghese F 2010 *ACS Nano* **4** 6369–76
- [9] Tame M S, McEnery K R, Özdemir Ş K, Lee J, Maier S A and Kim M S 2013 *Nature Phys.* **9** 329–40
- [10] Henzie J, Lee J, Lee M H, Hasan W and Odom T W 2009 *Ann. Rev. Phys. Chem.* **60** 147–65
- [11] Mühlig S, Cunningham A, Dintinger J, Scharf T, Bürgi T, Lederer F and Rockstuhl C 2013 *Nanophotonics* **2** 211–40
- [12] Jensen L, Aikens C M and Schatz G C 2008 *Chem. Soc. Rev.* **37** 1061–73
- [13] Apell P and Penn D R 1983 *Phys. Rev. Lett.* **50** 1316
- [14] Apell P, Ljungbert A and Lundqvist S 1984 *Phys. Scr.* **30** 367–83
- [15] Lassiter J B, Aizpurua J, Hernandez L I, Brandl D W, Romero I, Lal S, Hafner J H, Nordlander P and Halas N J 2008 *Nano Lett.* **8** 1212
- [16] Stella L, Zhang P, García-Vidal F J, Rubio A and García-González P 2013 *J. Phys. Chem. C* **117** 8941–9
- [17] Zuloaga J, Prodan E and Nordlander P 2009 *Nano Lett.* **9** 887–91
- [18] Zuloaga J, Prodan E and Nordlander P 2010 *ACS Nano* **4** 5269–76
- [19] McMahon J M, Gray S K and Schatz G C 2010 *Phys. Rev. B* **82** 035423
- [20] Morton S M, Silverstein D W and Jensen L 2011 *Chem. Rev.* **111** 3962–94
- [21] Teperik T V, Nordlander P, Aizpurua J and Borisov A G 2013 *Phys. Rev. Lett.* **110** 263901
- [22] Wu X, Gray S K and Pelton M 2010 *Opt. Express* **18** 23633–45
- [23] Esteban R, Borisov A G, Nordlander P and Aizpurua J 2012 *Nature Commun.* **3** 825
- [24] McMahon J M, Gray S K and Schatz G C 2010 *J. Phys. Chem. C* **114** 15903–8
- [25] Corni S and Tomasi J 2001 *J. Chem. Phys.* **114** 3739
- [26] Lopata K and Neuhauser D 2009 *J. Chem. Phys.* **130** 104707
- [27] Masiello D J and Schatz G C 2008 *Phys. Rev. A* **78** 042505
- [28] Chen H, McMahon J M, Ratner M A and Schatz G C 2010 *J. Phys. Chem. C* **114** 14384–92
- [29] Morton S M and Jensen L 2010 *J. Chem. Phys.* **133** 074103

- [30] Gersten J and Nitzan A 1980 *J. Chem. Phys.* **73** 3023
- [31] Barnes W L 1998 *J. Mod. Opt.* **45** 661
- [32] Chen H, Schatz G C and Ratner M A 2012 *Rep. Prog. Phys.* **75** 096402
- [33] Mullin J and Schatz G C 2012 *J. Phys. Chem. A* **116** 1931–8
- [34] Payton J L, Morton S M, Moore J E and Jensen L 2012 *J. Chem. Phys.* **136** 214103
- [35] Trügler A and Hohenester U 2008 *Phys. Rev. B* **77** 115403
- [36] Manjavacas A, García de Abajo F J and Nordlander P 2011 *Nano Lett.* **11** 2318–23
- [37] Masiello D J and Schatz G C 2010 *J. Chem. Phys.* **132** 064102
- [38] Morton S M and Jensen L 2011 *J. Chem. Phys.* **135** 134103
- [39] Coomar A, Arntsen C, Lopata K A, Pistinner S and Neuhauser D 2011 *J. Chem. Phys.* **135** 084121
- [40] Gao Y and Neuhauser D 2012 *J. Chem. Phys.* **137** 074113
- [41] Bellessa J, Bonnand C, Plenat J C and Mugnier J 2004 *Phys. Rev. Lett.* **93** 036404
- [42] Fofang N T, Grady N K, Fan Z, Govorov A O and Halas N J 2011 *Nano Lett.* **11** 1556–60
- [43] Walter M, Häkkinen H, Lehtovaara L, Puska M, Enkovaara J, Rostgaard C and Mortensen J J 2008 *J. Chem. Phys.* **128** 244101
- [44] Enkovaara J et al 2010 *J. Phys.: Condens. Matter* **22** 253202
- [45] Yee K S 1966 *IEEE Trans. Antennas Propag.* **14** 302
- [46] Taflove A and Hagness S 2005 *Computational Electrodynamics: the Finite-Difference Time-Domain Method* 3rd edn (Norwood, MA: Artech House)
- [47] Larsson J 2007 *Am. J. Phys.* **75** 230
- [48] Gao Y and Neuhauser D 2013 *J. Chem. Phys.* **138** 181105
- [49] Li S, Gao Y and Neuhauser D 2012 *J. Chem. Phys.* **136** 234104
- [50] Runge E and Gross E K U 1984 *Phys. Rev. Lett.* **52** 997
- [51] Castro A, Marques M A L and Rubio A 2004 *J. Chem. Phys.* **121** 3425–33
- [52] Chelikowsky J R, Troullier N and Saad Y 1994 *Phys. Rev. Lett.* **72** 1240–3
- [53] Blöchl P E 1994 *Phys. Rev. B* **50** 17953
- [54] Mortensen J J, Hansen L B and Jacobsen K W 2005 *Phys. Rev. B* **71** 035109
- [55] Gabovich A M, Gunko V M, Klymenko V E and Voitenko A I 2012 *Eur. Phys. J. B* **85** 284
- [56] Yabana K and Bertsch G F 1996 *Phys. Rev. B* **54** 4484–7
- [57] Pitarke J M, Silkin V M, Chulkov E V and Echenique P M 2007 *Rep. Prog. Phys.* **70** 1–87
- [58] Bernadotte S, Evers F and Jacob C R 2013 *J. Phys. Chem. C* **117** 1863–78
- [59] Malola S A, Lehtovaara L, Enkovaara J and Häkkinen H 2013 *ACS Nano* **7** 10263
- [60] West P R, Ishii S, Naik G V, Emami N K, Shalae V M and Boltasseva A 2010 *Laser Photon. Rev.* **4** 795–808
- [61] Lu L, Burkey G, Halaciuga I and Goia D V 2013 *J. Colloid Interface Sci.* **392** 90–5
- [62] Yan J, Yuan Z and Gao S 2007 *Phys. Rev. Lett.* **98** 216602
- [63] Yan J and Gao S 2008 *Phys. Rev. B* **78** 235413
- [64] Wang S, Boussaad S and Tao N J 2001 *Rev. Sci. Instrum.* **72** 3055
- [65] Ataka K and Heberle J 2007 *Anal. Bioanal. Chem.* **388** 47–54
- [66] Pettinger B, Schambach P, Villagómez C J and Scott N 2012 *Ann. Rev. Phys. Chem.* **63** 379–99
- [67] Li J F et al 2013 *Nature Protoc.* **8** 52–65
- [68] King P W, Van Duyne R P and Schatz G C 1978 *J. Chem. Phys.* **69** 4472
- [69] De Giovannini U, Brunetto G, Castro A, Walkenhorst J and Rubio A 2013 *Chem. Phys. Chem.* **14** 1363–76
- [70] Senn H M and Thiel W 2009 *Angew. Chem. Int. Edn Engl.* **48** 1198–229
- [71] Datta S and McLennan M J 1990 *Rep. Prog. Phys.* **53** 1003
- [72] Arnold A and Jüngel A 2006 *Analysis, Modeling and Simulation of Multiscale Problems* ed A Mielke (Heidelberg: Springer) p 331–63
- [73] Ojanperä A, Havu V, Lehtovaara L and Puska M 2012 *J. Chem. Phys.* **136** 144103
- [74] Marinica D C, Lourenço-Martins H, Aizpurua J and Borisov A G 2013 *Nano Lett.* **13** 5972